Published in final edited form as:
Magn Reson Imaging. 2009 December ; 27(10): 1309–1318. doi:10.1016/j.mri.2009.05.032.

MRI-based biomechanical imaging: initial study on early plaque progression and vessel remodeling

Jie Zheng[a,*], **Dana R. Abendschein**[a], **Ruth J. Okamoto**[a], **Deshan Yang**[a], **Kyle S. McCommis**[a], **Bernd Misselwitz**[b], **Robert J. Gropler**[a], and **Dalin Tang**[c]

[a]Mallinckrodt Institute of Radiology, Washington University, St. Louis, MO 63131, USA

[b]Bayer Schering Pharma AG, 13353 Berlin, Germany

[c]Worcester Polytechnic Institute, MA 01609, USA

Abstract

The goal of the study is to develop a noninvasive magnetic resonance imaging (MRI)-based biomechanical imaging technique to address biomechanical pathways of atherosclerotic progression and regression in vivo using a 3D fluid-structure interaction (FSI) model. Initial in vivo study was carried out in an early plaque model in pigs that underwent balloon-overstretch injury to the left carotid arteries. Consecutive MRI scans were performed while the pigs were maintained on high cholesterol (progression) or normal chow (regression), with an injection of a plaque-targeted contrast agent, Gadofluorine M. At the end of study, the specimens of carotid arterial segments were dissected and underwent dedicated mechanical testing to determine their material properties. 3D FSI computational model was applied to calculate structure stress and strain distribution. The plaque structure resembles early plaque with thickened intima. Lower maximal flow shear stress correlates with the growth of plaque volume during progression, but not during regression. In contrast, maximal principle structure stress/stain (stress-P1 and strain-P1) were shown to correlate strongly with the change in the plaque dimension during regression, but moderately during progression. This MRI-based biomechanical imaging method may allow for noninvasive dynamic assessment of local hemodynamic forces on the development of atherosclerotic plaques in vivo.

Keywords

MR; Atherosclerosis; Biomechanics; Stress; Stain; Contrast agent

1. Introduction

Atherosclerosis is first formed by thickened intima that responses to chronic arterial injury. The subsequent plaque progression depends upon the plaque growth and/or vascular remodeling. The focal and eccentric nature of atherosclerotic plaques are well recognized [1–3] as the plaques often form at regions near bifurcations, bends and branch ostia. These complicated events involve a cascade of molecular and cellular processes that characterize the activation of vascular endothelial cells and platelets, recruitment of leukocytes through expression of cellular adhesion molecules (e.g., $\alpha_v\beta_3$ integrins, selectins, proteoglycans,

*Corresponding author. Mallinckrodt Institute of Radiology, Washington University School of Medicine, Box 8225, St. Louis, MO 63110, USA. Tel.: +1 314 747 4608; fax: +1 314 747 3882. zhengj@mir.wustl.edu (J. Zheng)..

etc.), increased vascular permeability to lipoproteins, smooth muscle cell (SMC) proliferation, increased endothelial cell apoptosis and altered hemostatic and fibrinolytic balances for thrombogenesis. Although many systemic factors such as hypertension, smoking, hyperlipidemia and diabetes mellitus have profound impacts on endothelial cell function and plaque progression [4], local biomechanical factors such as flow-generated shear stress (SS) have been identified to influence remarkably the formation, remodeling, and progression of vascular plaque through the activities of local mechanotransduction mechanisms [5].

The commonly held concept is that low or oscillatory flow SS promotes the development of early fibroatheromas while higher physiologic SS activates various atheroprotective genes on endothelial cells, leading to the stability of the plaque [6]. Cheng et al. [7] designed a unique taped polymeric cast to induce low and high shear stress around one carotid artery of $ApoE^{-/-}$ mice. Significantly larger plaque was observed in the region of low SS with intraplaque hemorrhage. In a progression study with a coronary plaque porcine model [8], lower SS was associated with high-risk plaques, characterized by lipid accumulation, inflammation, thin fibrous cap, severe internal elastic lamina degradation and excessive expansive remodeling. Serial in vivo study in patients with coronary artery disease (CAD), by using the intravascular ultrasound imaging technique (IVUS), has also demonstrated strong correlation between regions of low SS, and the sites exhibited coronary plaque progression and expansive remodeling [9]. Using the same imaging technique, however, Fukumoto et al [10] show localized high SS is related to plaque rupture in vivo, but the flow SS appears to have no effect on plaque regression from lipid lowering therapy [11]. Recently, study in carotid artery with relatively severe stenosis by Tang et al. [12] pinpointed that structure tensile stress within the plaque, in addition to flow SS, may also play an important role in the regulation of plaque progression and vulnerability. No study has been reported so far to exam the impact of both structure stress and SS on the progression and regression of early plaques.

Gadofluorine M. (Bayer Schering Pharma, Berlin, Germany) enhanced magnetic resonance imaging (MRI) plaque images have been reported in animal atherosclerosis models such as rabbits and swine [13–15]. Recent research using fluorescence imaging techniques has revealed that Gadofluorine M. strongly attaches to several extracellular matrix (ECM) components: collagen, elastin, proteoglycans and tenascins but has much lower affinity for normal media, lipids and macrophages [16]. Because early plaque is characterized by adaptive intimal thickening and the intimal xanthoma consists of SMCs and ECM, Gadofluorine M. maybe one of ideal contrast agents to aid in the visualization of early plaques by MRI. In this project, a single- or double-injury atherosclerotic plaque model in pigs was used to simulate the early plaque phenotype. The purpose of this investigation is to seek how stress and strain affect the progression and regression of early plaque, as well as concomitant vascular remodeling.

2. Materials and methods

2.1. Animal preparation and artery injury

Three Yucatan mini-pigs (weight=33±4 kg) were used in this initial in vivo study. A baseline blood sample was first obtained for measurement of serum lipid profile. The pigs were first fed an high cholesterol (HC) diet (modified porcine 4% cholesterol w/apple flavor diet, Purina Mills Test Diet, Richmond, IN, USA) for approximately 2 weeks. Once their total cholesterol levels increased to over 200 mg/dl, the pigs underwent the first carotid artery injury via balloon over inflation. Two of the three pigs also received a second balloon overstretch injury at the same arterial segment as the first injury. All of injuries were performed in the left carotid artery, between the second and fourth cervical vertebra (Fig. 1).

The right carotid arteries served as the control cases. All animal techniques were approved by the animal study committee of our institute.

For the surgical injury of the vessels, an ear vein was first cannulated and normal saline was administered. The trachea was intubated, and inhaled isofluorine (1–3%) was used to maintain anesthesia. An 8F catheter sheath was inserted into the exposed right femoral artery. Baseline carotid artery angiography was first performed and a balloon catheter (Proflex 5, 8×2 mm, Mallinckrodt, St. Louis, MO, USA) was advanced into the left carotid artery to the level of the second or third cervical vertebrae. The balloon was inflated five times to a distending pressure of 8 atm for 30 s with 60 s between inflations. Our previous experience [17] has shown consistent disruption of the internal elastic lamina by this method. The second injury repeated the same procedure on the first injury site, as confirmed by fluoroscopic images.

2.2. Experimental protocol

Pig 1 was injured only once and was scanned twice by MRI: at 10 and 14 weeks after the injury for progression study. Pigs 2 and 3 underwent two carotid artery injuries aiming to create more aggressive atherosclerotic plaques. Four MRI scans at time points 1–4 (T1–T4) were performed on these two pigs to monitor plaque development (Fig. 1). The HC diet was maintained for all progression studies, then normal porcine chow was fed between the third and fourth MRI scans, for the purpose of imaging plaque regression.

The MRI scans were performed on a 3T Trio MRI System (Siemens Medical Solutions, Malvern, PA, USA). Hemodynamic data was recorded every 15 min while under anesthesia with isofluorine (1.5–2%); 0.075 mmol/kg Gadofluorine M. was injected intravenously 1 h prior to all scans. The MRI protocol consisted of 20-slice T_1-weighted (T_1w) and T_2-weighted (T_2w) and imaging using a dark-blood (DB) turbo-spin-echo sequence, as well as 20-slice 3D time-of-flight (TOF) imaging. DB images were achieved using superior and inferior presaturation bands. A spectral fat saturation pulse was used to suppress signals from periadventitial fat. For T_1w imaging, the data acquisition parameters included: TR/TE=600/13 ms, field of view=160×160 cm, interpreted matrix size=896×896, interpolated pixel size=180×180 μm, and signal average=8. For the T_2w images, TR/TE=2400/40 ms, acquisition time=20 min. For TOF, TR/TE=15/4.6 ms, flip angle=20°. All imaging slice thickness was 2 mm. It was found in our initial studies (unpublished data) that T_1w images produced the best delineation of the outer boundary of the vessel wall, whereas T_2w images showed the highest contrast in the Gadofluorine M.-enhanced area. TOF images were particularly helpful in delineating the lumen area with bright blood signal intensity.

2.3. Histopathology

After the completion of all MRI studies, the chests of the pigs were opened through median sternotomy. The superior and inferior vena cava and the left subclavian artery were ligated with braided nylon ties. Saline (200 ml) was perfused through an aortic catheter to the carotid arteries in situ at physiologic pressure (100 mm Hg). Both normal right and left injured carotid artery segments were removed (approximately 3 cm in length). The center piece of each segment (approximately 1 cm in length) was cut and immediately sent to the mechanical testing laboratory. The rest of the artery was fixed in 4% paraformaldehyde fixative for 24 h and cut at 2-mm intervals to match the corresponding MR images. These sections were embedded in paraffin, step cross-sectioned (5-μm thickness) at 100-μm intervals, and stained with hematoxylin and eosin and Verhoffs van Gieson stains.

2.4. Mechanical testing

The protocol for standard planar biaxial testing is similar to that described by Okamoto et al. [18]. In brief, connective tissue on the adventitial surface of the carotid artery segment was first removed using a dissecting microscope, and an axial cut was made along the length of the artery. The specimen was bathed in a calcium-free physiologic salt solution with 0.1 mM papaverine. The segment was then opened, and the rectangular segment was sutured on all four sides with continuous lengths of 6-0 silk suture. After suturing, four small markers forming a quadrilateral (1–2 mm per side) were glued to the intima in the central region of the specimen using cyanoacrylate glue. These markers were used to track tissue deformations with a video system, while force was measured in the axial and circumferential directions. Force displacement data from the strip biaxial tests (i.e., one direction will be stretched while the other direction was held at a constant length) and an equibiaxial stretching test was converted to stress-stretch data that were used to determine the mechanical properties of injured carotids and contralateral controls. This was done by fitting material parameters in an exponential, isotropic strain energy density function [19]:

$$W = c_1 (I_1 - 3) + c_2 (I_2 - 3) + D_1 \{\exp [D_2 (I_1 - 3)] - 1\} \quad (1)$$

where W is the strain energy per unit volume, $\{c_1, c_2, D_1, D_2\}$ are the parameters describing the material behavior and I_1 and I_2 are the first and second invariants of C.

2.5. Image analysis

To segment the plaque images into different components, we applied a 3D multicontrast, contour-based segmentation software developed at our institute [20]. The segmentation algorithm in this software is based on both clustering methods and an active deformable model (level set). Because our plaque images were acquired post-contrast using a ECM-targeting agent, Gadofluorine M., the enhanced areas are closely associated with ECM that was found to be the major plaque component in this porcine atherosclerotic model. Based on these features, we first manually defined the contour of the outer boundary in the T_1w images and then automatically delineated the contour of the lumen using the level set segmentation method on TOF images. The right normal carotid artery vessel wall was segmented using this approach and the average signal intensity (SI) and S.D. of the entire wall area on T_2w images were obtained for every slice. Since the normal vessel wall was not enhanced by Gadofluorine M., a thresholding value of SI+2×S.D. was used for the segmentation of the left enhanced plaque wall area in the same slice on T_2w images. Representative MR images and segmented plaque wall images are shown in Fig. 2. Notably, the motion between three MR contrast images was minimal in the controlled animal study and could be corrected manually by the software if any drift was observed.

2.6. Computational modeling

3D MRI data sets consisting of 2D slices (20 slices) from pig arteries with high resolution ($0.18 \times 0.18 \times 2$ mm^3) were segmented with the 3D segmentation software. 3D plaque geometry and mesh were then reconstructed following the previously described procedure [21]. A multicomponent computational model FSI was applied to calculate the stress and strain distributions in the plaque and wall area. For the solid models, both artery wall and plaque components were assumed to be hyperelastic, isotropic, incompressible and homogeneous. The modified Mooney-Rivlin (M-R) model was used to describe the nonlinear material properties of the vessel wall and plaque components with parameters from mechanical testing. Approximate pressure conditions were set using cuffed pressure data from the pigs. Incremental steps were taken so that the artery was stretched (axially) and pressurized gradually to specified conditions. The same solid model was used for all

artery and plaque components except that different material parameters were selected for each material. The strain energy function for the modified M-R model is given by Eq. (1).

The coupled fluid and structure models were solved by a commercial finite-element package ADINA (ADINA R & D, Watertown, MA, USA). Proper mesh was chosen to fit the shape of each plaque component, the vessel and the fluid domain. Nonlinear incremental iterative procedures were used to handle fluid-structure interactions. The governing finite element equations for both the solid and fluid models were solved by the Newton-Raphson iteration method [22]. Details of the computational models and solution methods are given in Ref. [23]. The initial material parameters in the M-R model were previously defined [24,25]. The final material parameters were determined by using the least-square method to match the stress-strain behavior obtained in mechanical testing to the degree of arterial stenosis. Stress and strain are tensors with six components each at each pixel of the plaque areas. For the sake of clarity, maximal flow SS, stress-P1 and strain-P1 were used for further data analysis. Fig. 3A demonstrates longitudinal view of constructed flow SS and stress-P1 maps.

2.7. Data analysis

Geometry data measured from MR images, including mean vessel wall area (VWA), contrast-enhanced areas, fibrotic tissue areas, lumen size, etc., were obtained and compared at different time points with a repeated analysis of variance. Wall remodeling (WR) was calculated as:

$$\text{WR}=\text{Mean Plaque cross areas}/\text{Reference cross section} \quad (2)$$

Positive and negative remodeling index were defined as the WR>1 or <1, respectively. The proximal reference cross section was determined as the difference between the reference area and the mean area of the right normal artery is within three standard deviations of the right artery.

Stress-P1, strain-P1 and maximal flow SS were analyzed by correlating them with the increase in wall slice thickness. To do this, 60 data points were evenly selected in each slice on its lumen surface to track the wall thickness increase (WTI) over time (Fig. 3B). The corresponding stress and strain data on the lumen surface were recorded at these locations. Between T1 and T2, the Pearson correlations between stress-P1/strain-P1 at the T1 with WTI were calculated. In addition, we have adopted a similar analysis method as reported by Stone et al. [26] by dividing each variable into different categories. For example, stress-P1 can be divided into Categories 1, 2, 3, etc., with the difference in magnitude of 9 dyne/cm^2. For maximal flow SS, the difference was 6 dyne/cm^2, and for strain-P1, it was 0.02. For each category, the WTI was provided as mean±S.D. In this way, the effect of each stress and strain component could be readily visualized as the change in plaque size. The Spearman rank-order correlation coefficients were calculated as a quantitative measure.

3. Results

3.1. Morphology changes of the vessel wall

The weight of Pig 1 increased from 28.6 kg (T1) to 31.8 kg (T2) in 1 month, whereas the mean weight of Pig 2 and 3 increased from 35.4±1.3 kg (T1) to 70.5±3.2 kg (T4) during a 7-month study. There are 16, 9 and 12 matching slices for Pigs 1, 2 and 3, respectively. The parameters from these slices were used for all of following analysis. Fig. 4 shows the morphologic changes in the carotid arteries in three pigs. In Pig 1 (Fig. 4A), significant increases in the mean VWA and lumen were observed in the left injured artery during the 4-

week progression, whereas the normal right artery maintained the same dimension. There was compensatory enlargement of the left arterial lumen due to the plaque burden on the left carotid artery.

From the combined results of Pigs 2 and 3, at four time points (Fig. 4B), the mean VWA of left carotid arterial wall increased significantly from T1 to T2 (16.5%, $P<.01$) and then decreased (−15.9%, $P<.001$) from Scan 3 to Scan 4, whereas the mean lumen area trended towards a gradual increase (7.8%, $P<.01$, and 2.1%, P=NS, respectively). In contrast, the VWA of the right normal carotid artery decreased slightly from T1 to T2 (−2.2%, P=NS) and significantly from T3 to T4 (−24.0%, $P<.001$). In both time periods, the lumen of right carotid artery changed slightly, −6.3% ($P<.05$) and 0.3% (P=NS), respectively.

The VWA of the left carotid artery consists of enhanced and non-enhanced areas (Fig. 3C). Interestingly, the enhanced area dramatically increased 46.6% ($P<.02$) during the progression period and then sharply decreased 36% ($P<.001$). In contrast, nonenhanced area merely increased 9.6% ($P=.054$) during the progression period and decreased 4% ($P=.051$) during the regression period. This may be explained by the reduction of the fatty diet significantly reducing the neointimal component and converting the plaque to a more fibrotic plaque.

3.2. Mechanical testing

There are significant differences in the mechanical properties of normal carotid arteries and arteries with induced atherosclerosis. Fig. 5 shows relationships of stress versus strain in the axial direction in Pig 3. These differences appear to be more prominent in the axial direction than in the circumferential direction (data not shown). No consistent findings in the material properties are observed for either normal or diseased carotid vessels, further emphasizing the importance of the measurement of subject-specific mechanical properties.

3.3. Computational results

The findings of the flow SS, stress-P1 and strain-P1 are shown in Fig. 6. A lower flow SS leads to a larger change in WT during the progression period, whereas the association of WT with flow SS varied in Pigs 2 and 3. In contrast, there is no association of stress-P1 with WT from T1 to T2 (Fig. 6C), but low stress-P1 clearly leads to reduced WT (Fig. 6D) from T3 to T4. Similar trends were observed for strain-P1 (Fig. 6E and F).

With Gadofluorine M. enhancement, the relatively large plaque could be differentiated into two components: enhanced and nonenhanced ones. The Spearman correlation coefficients and corresponding P values are shown in Table 1. Flow SS appears to have a strong effect on the non-enhanced component, whereas the enhanced component may be affected mostly by the stress-P1 and strain-P1. The bold data highlights those with significant P values.

3.4. Vessel wall remodeling

The findings on the WR of the left artery are summarized in Table 2. The data demonstrate excessive expansive remodeling in the injured artery during the progression period and even continue during the short regression period. Combining data from both Pigs 2 and 3, there is strong positive correlation between the mean WT of all slices and WR during the progression time (R^2=0.7). However, this correlation is weak during the regression time (R^2=0.2). The correlation between the changes in mean WT and changes in WR is also mild (R^2=0.3). There are no consistent correlations between any baseline hemodynamic parameters (stress-P1, strain-P1 or flow SS) and the changes in WR or mean WT.

4. Discussion

The effects of local hemodynamic forces on plaque progression and ultimate rupture have long been recognized [27–29]. The blood flow-induced shear stress remains on the center stage due to its fundamental role on atherosclerosis [30] and continues to be an intensive research topic in the cause and risk stratification of atherosclerotic disease. Although blood pressure-derived tensile stress has also been recognized for its impacts on plaque development, the limitation of the direct measurements of tensile stress in vivo has hindered further investigation of its role in plaque development. Recent advances in 3D computational modeling open a new venue for this purpose [31], but the results depend on some assumed material properties. In this pilot study, we for the first time demonstrate an approach with integration of MRI and 3D modeling to comprehensively investigate the hemodynamic forces in an early plaque animal model. From this longitudinal study, we have found comparable results of flow shear stress with other reports [6–8]. Furthermore, we have clearly demonstrated tensile stress and strain also play important roles in plaque development. Specifically, low principle stress and strain promote plaque regression and prevent plaque progression (Fig. 7). Some findings in this animal study are correlated well with other ongoing study in human carotid atherosclerosis [12].

Accurate delineation of plaque morphology is pivotal for the accurate calculation of mechanical forces using the 3D modeling method. We have used a plaque-specific contrast agent, Gadofluorine M., to highlight the plaque and further differentiate two plaque components: the fibrous tissue and the neointima in this model. This agent was investigated thoroughly in a rabbit atherosclerosis model and was shown to diffuse into the plaque and then bind with ECM proteins, including collagens, proteoglycans and tenascin [16]. Since the neointima in this angioplasty injury model mostly consists of ECM and few macrophage cells, we have found strong T_1-weigthed signal enhancement in the neointimal portion of the plaque. In this three-pig study, one pig shows relatively large amounts of neointima that can be readily seen by MRI, as validated by histopathology. Due to the spatial resolution limits, in the other two pigs, the much smaller neointima layer cannot be appreciated by MRI, except for the enlarged media due to vascular inflammation. This observation, along with another study in rabbits [32], further confirms that Gadofluorine M. may be well suited for the detection of early atherosclerotic plaque.

Local hemodynamic forces generated by pulsatile blood flow have been demonstrated to lead to endothelial dysfunction with stress response promoter elements and transcription factors [33]. The mechanopathogenesis of atherosclerosis was recently reviewed in detail by VanEpps et al [5]. Low and oscillatory flow SS may regulate endothelial gene expression through a cascade of intracellular signal transduction events (local mechanotransduction mechanisms) that eventually promote the initialization and progression of early atherosclerosis. In contrast, physiologic flow SS appears to have protective effects that limit vessel inflammation [5]. Our calculated flow SS findings in three pigs clearly show the same conclusion that lower flow SS is associated with larger plaque wall thicknesses during plaque progression. This observation partially validates our MRI-based computational modeling. Absolute flow SS values are spanned from 10–82 dyne/cm^2, which is in agreement with physiologic flow SS values (15–70 dyne/cm^2) in human carotid arteries [33]. After regression, the wall remodeling index was reduced from 1.33 to 1.29 (P=.007) for Pigs 2 and 3, indicating a constrictive remodeling. This finding is consistent with the Reversal of Atherosclerosis with Aggressive Lipid Lowering study performed in human coronary artery with lipid lowering therapy [34]. It was suggested that lower flow SS may not have a direct impact in on the pathobiology of constrictive remodeling [35]. In our study, although Pig 3 in Fig. 6B shows similar SS-wall-thickness pattern during progression, Pig 2 shows no effect of flow SS. Therefore, the effect of flow SS is inconclusive in this study. A

comprehensive investigation with a larger number of subjects is warranted to elucidate the role of SS when a plaque regresses.

For arterial structure stress (in 3D form) or tensile stress (in 2D form), it was found in an early study that reduced wall stress can restore the morphology of endothelial cells in the high-risk regions to normal, as seen in the low-risk regions [36]. Other studies have suggested a similar interactions between structure stress and cellular processes as flow SS [37]. Generally speaking, elevated structure stress modulates various atherogenic gene expressions that stimulate vascular SMC proliferation, increase reactive oxygen species and up-regulate proinflammatory cytokines (vascular cell adhesion molecules, tumor necrosis factor-α, macrophages, etc.) [38,39]. These processes precipitate the progression of atherosclerosis. In human carotid artery patients, Tang et al. [12] observed significant correlation between the progression of plaque wall thickness and structure stress. In this animal study, this correlation was also demonstrated in Fig. 6 during progression but is much stronger during regression initiated by return to normal chow diet. Lower structure stress and strain lead to reduced increases in wall thickness. This observation is more prominent to neointimal thickness than media thickness (Table 1) during regression. It is then postulated that, during lipid lowering therapy, plaque regions with lower structure stress will show the most benefit by significantly reduced neointimal plaque.

Expansive remodeling (WR >1) was observed in this animal model of atherosclerosis during progression. Increasing WT is associated with increased WR to preserve lumen size during the early plaque stage. Such positive correlation between WR and mean WT is consistent with Glagov's phenomenon [40] and other studies in animals [41,42],as well as in human coronary artery [43] with nonsignificant stenosis. Switching to normal diet (regression time) significantly reduced WR. Neointimal size correlated mostly with WR values. Lack of correlation between hemodynamic parameters and WR or mean WT may be due to the fact that all of these parameters are the “global” parameters, rather than those local parameters aforementioned (i.e., at one point of plaque surface). It is thus important to assess the local changes in plaque geometry and hemodynamic factors because of complex biomechanical milieu that occurred at different regions of atherosclerotic plaques, even within the same cross section.

4.1. Study limitations

The major limitation of this study is the small number of subjects. As a pilot study, our results have demonstrated initial evidence that integration of MRI, mechanical testing and 3D realistic computational FSI modeling could lead to more accurate measurements of plaque stress and strain. The heterogeneity of plaque formation and progression in these three pigs warrant future study with a larger sample size to validate our preliminary findings. Another limitation of this type of study is the lack of direct validation of the calculated plaque stress and strain. At least, consistent results in our flow SS with other reports indirectly validate our methodology on this part. There may be a need for developing certain in vivo measurements for the absolute quantifications of plaque stress and strain, but the changes in the stress and strain would still provide valuable insights to the mechanism of plaque development.

4.2. Clinical imprecation and conclusions

The approach in this study is expected to provide comprehensive biomechanical data to help elucidate the biomechanical pathways of plaque development. The quantitative information in this animal study is particularly important in terms of its application to the multifocal and heterogeneous lesions commonly found in CAD. For instance, acute coronary syndromes occurred at only a few of many local lesions that had low flow shear stress. Therefore, how

an individual coronary lesion develops in vivo is not yet fully understood. Furthermore, the animal study in this proposal provides guidance in terms of what degree of accuracy can be achieved by computational modeling in vivo since subject-specific material properties cannot be directly determined in vivo. For coronary artery lesions, because of the capability of high resolution images acquired by IVUS, Stone et al. [9] demonstrated the useful value of flow SS in the prediction of risks to coronary plaque during progression. With the knowledge we obtain from this animal study, we expect to develop hemodynamic models that might be able to comprehensively assess the risk of individual coronary artery lesions. Those that are identified to pose a future risk could then undergo a pre-emptive intervention in order to avert the adverse events. Furthermore, if the structure stress and strain are the dominant factors in biomechanics during plaque regression, one can make useful predictions which plaque may benefit from lipid-lowering therapy, based on the computational findings. Once noninvasive MRI techniques develop to the point at which it is able to differentiate major plaque components in coronary artery in vivo, the proposed approaches will permit truly noninvasive characterization of coronary artery plaque dynamically and also offer a valuable tool to monitor the effects of therapeutic interventions aimed at the stabilization and/or regression of the plaque.

Acknowledgments

The authors would like to thank Bayer Schering Pharma for providing the Gadofluorine M. contrast agent in this animal study. The authors also wish to thank Pamela Baum for her assistance with the animal procedures.

References

[1]. Badimon L, Badimon JJ, Cohen M, Chesebro JH, Fuster V. Vessel wall-related risk factors in acute vascular events. Drugs 1991;42:1–9. [PubMed: 1726211]

[2]. Shah PK, Forrester JS. Pathophysiology of acute coronary syndromes. Am J Cardiol 1991;68:16C–23C.

[3]. Berglund H, Luo H, Nishioka T, Fishbein MC, Eigler NL, Tabak SW, et al. Highly localized arterial remodeling in patients with coronary atherosclerosis: an intravascular ultrasound study. Circulation 1997;96:1470–6. [PubMed: 9315533]

[4]. Ehtisham A, Chimowitz MI, Furlan AJ, Lafranchise EF. Systemic risk factors associated with progression of atherosclerosis from the coronary to the carotid arteries. J Stroke Cerebrovasc Dis 2005;14:182–5. [PubMed: 17904023]

[5]. Vanepps JS, Vorp DA. Mechano-pathobiology of atherogenesis: a review. J Surg Res 2007;142:202–17. [PubMed: 17612564]

[6]. Cunningham KS, Gotlieb AI. The role of shear stress in the pathogenesis of atherosclerosis. Lab Invest 2005;85:9–23. [PubMed: 15568038]

[7]. Cheng C, Tempel D, van Haperen R, van der Baan A, Grosveld F, Daemen MJ, et al. Atherosclerotic lesion size and vulnerability are determined by patterns of fluid shear stress. Circulation 2006;113:2744–53. [PubMed: 16754802]

[8]. Chatzizisis YS, Jonas M, Coskun AU, Beigel R, Stone BV, Maynard C, et al. Prediction of the localization of high-risk coronary atherosclerotic plaques on the basis of low endothelial shear stress: an intravascular ultrasound and histopathology natural history study. Circulation 2008;117:993–1002. [PubMed: 18250270]

[9]. Stone PH, Coskun AU, Kinlay S, Popma JJ, Sonka M, Wahle A, et al. Regions of low endothelial shear stress are the sites where coronary plaque progresses and vascular remodelling occurs in humans: an in vivo serial study. Eur Heart J 2007;28:705–10. [PubMed: 17347172]

[10]. Fukumoto Y, Hiro T, Fujii T, Hashimoto G, Fujimura T, Yamada J, et al. Localized elevation of shear stress is related to coronary plaque rupture: a 3-dimensional intravascular ultrasound study with in-vivo color mapping of shear stress distribution. J Am Coll Cardiol 2008;51:645–50. [PubMed: 18261684]

[11]. Wentzel JJ, Corti R, Fayad ZA, Wisdom P, Macaluso F, Winkelman MO, et al. Does shear stress modulate both plaque progression and regression in the thoracic aorta? Human study using serial magnetic resonance imaging. J Am Coll Cardiol 2005;45:846–54. [PubMed: 15766817]

[12]. Tang D, Yang C, Mondal S, Liu F, Canton G, Hatsukami TS, et al. A negative correlation between human carotid atherosclerotic plaque progression and plaque wall stress: In vivo MRI-based 2D/3D FSI models. J Biomech 2008;41:727–36. [PubMed: 18191138]

[13]. Sirol M, Itskovich VV, Mani V, Aguinaldo JG, Fallon JT, Misselwitz B, et al. Lipid-rich atherosclerotic plaques detected by gadofluorine-enhanced in vivo magnetic resonance imaging. Circulation 2004;109:2890–6. [PubMed: 15184290]

[14]. Koktzoglou I, Harris KR, Tang R, Kane BJ, Misselwitz B, Weinmann HJ, et al. Gadofluorine-enhanced magnetic resonance imaging of carotid atherosclerosis in Yucatan miniswine. Invest Radiol 2006;41:299–304. [PubMed: 16481913]

[15]. Zheng J, Ochoa E, Misselwitz B, Yang D, El Naqa I, Woodard PK, et al. Targeted contrast agent helps to monitor advanced plaque during progression: a magnetic resonance imaging study in rabbits. Invest Radiol 2008;43:49–55. [PubMed: 18097277]

[16]. Meding J, Urich M, Licha K, Reinhardt M, Misselwitz B, Fayad ZA, et al. Magnetic resonance imaging of atherosclerosis by targeting extracellular matrix deposition with Gadofluorine M. Contrast Media Mol Imaging 2007;2:120–9. [PubMed: 17557276]

[17]. St Pierre J, Yang LY, Tamirisa K, Scherrer D, De Ciechi P, Eisenberg P, et al. Tissue factor pathway inhibitor attenuates procoagulant activity and upregulation of tissue factor at the site of balloon-induced arterial injury in pigs. Arterioscler Thromb Vasc Biol 1999;19:2263–8. [PubMed: 10479671]

[18]. Okamoto RJ, Wagenseil JE, DeLong WR, Peterson SJ, Kouchoukos NT, Sundt TM III. Mechanical properties of dilated human ascending aorta. Ann Biomed Eng 2002;30:624–35. [PubMed: 12108837]

[19]. Tang D, Yang C, Zheng J, Woodard PK, Saffitz JE, Sicard GA, et al. Local maximal stress hypothesis and computational plaque vulnerability index for atherosclerotic plaque assessment. Ann Biomed Eng 2005;33:1789–801. [PubMed: 16389527]

[20]. El Naqa I, Yang D, Apte A, Khullar D, Mutic S, Zheng J, et al. Concurrent multimodality image segmentation by active contours for radiotherapy treatment planning. Med Phys 2007;34:4738–49. [PubMed: 18196801]

[21]. Tang D, Yang C, Zheng J, Woodard PK, Saffitz JE, Sicard GA, et al. Quantifying effects of plaque structure and material properties on stress distributions in human atherosclerotic plaques using 3D FSI models. J Biomech Eng 2005;127:1185–94. [PubMed: 16502661]

[22]. Deuflhard, P. Springer Series in Computational Mathematics. Vol. Vol. 35. Springer; Berlin: 2004. Newton methods for nonlinear problems. Affine invariance and adaptive algorithms.

[23]. Tang D, Yang C, Kobayashi S, Zheng J, Vito RP. Effect of stenosis asymmetry on blood flow and artery compression: a three-dimensional fluid-structure interaction model. Ann Biomed Eng 2003;31:1182–93. [PubMed: 14649492]

[24]. Huang H, Virmani R, Younis H, Burke AP, Kamm RD, Lee RT. The impact of calcification on the biomechanical stability of atherosclerotic plaques. Circulation 2001;103:1051–6. [PubMed: 11222465]

[25]. Williamson SD, Lam Y, Younis HF, Huang H, Patel S, Kaazempur-Mofrad MR, et al. On the sensitivity of wall stresses in diseased arteries to variable material properties. J Biomech Eng 2003;125:147–55. [PubMed: 12661209]

[26]. Stone PH, Coskun AU, Kinlay S, Clark ME, Sonka M, Wahle A, et al. Effect of endothelial shear stress on the progression of coronary artery disease, vascular remodeling, and in-stent restenosis in humans: in vivo 6-month follow-up study. Circulation 2003;108:438–44. [PubMed: 12860915]

[27]. Chien S, Li S, Shyy YJ. Effects of mechanical forces on signal transduction and gene expression in endothelial cells. Hypertension 1998;31:162–9. [PubMed: 9453297]

[28]. Chatzizisis YS, Giannoglou GD. Coronary hemodynamics and atherosclerotic wall stiffness: a vicious cycle. Med Hypotheses 2007;69:349–55. [PubMed: 17343988]

[29]. Korshunov VA, Schwartz SM, Berk BC. Vascular remodeling: hemodynamic and biochemical mechanisms underlying Glagov's phenomenon. Arterioscler Thromb Vasc Biol 2007;27:1722–8. [PubMed: 17541029]

[30]. Siasos G, Tousoulis D, Siasou Z, Stefanadis C, Papavassiliou AG. Shear stress, protein kinases and atherosclerosis. Curr Med Chem 2007;14(14):1567–72. [PubMed: 17584064]

[31]. Tang D, Yang C, Zheng J, Woodard PK, Sicard GA, Saffitz JE, et al. 3D MRI-based multicomponent FSI models for atherosclerotic plaques. Ann Biomed Eng 2004;32(7):947–60. [PubMed: 15298432]

[32]. Barkhausen J, Ebert W, Heyer C, Debatin JF, Weinmann HJ. Detection of atherosclerotic plaque with Gadofluorine-enhanced magnetic resonance imaging. Circulation 2003;108:605–9. [PubMed: 12835227]

[33]. Ku DN, Giddens DP, Zarins CK, Glagov S. Pulsatile flow and atherosclerosis in the human carotid bifurcation. Positive correlation between plaque location and low oscillating shear stress. Arteriosclerosis 1985;5:293–302. [PubMed: 3994585]

[34]. Sipahi I, Tuzcu EM, Schoenhagen P, Nicholls SJ, Crowe T, Kapadia S, et al. Static and serial assessments of coronary arterial remodeling are discordant: an intravascular ultrasound analysis from the Reversal of Atherosclerosis with Aggressive Lipid Lowering (REVERSAL) trial. Am Heart J 2006;152:544–50. [PubMed: 16923429]

[35]. Chatzizisis YS, Coskun AU, Jonas M, Edelman ER, Feldman CL, Stone PH. Role of endothelial shear stress in the natural history of coronary atherosclerosis and vascular remodeling: molecular, cellular, and vascular behavior. J Am Coll Cardiol 2007;49:2379–93. [PubMed: 17599600]

[36]. Baker JW, Thubrikar MJ, Parekh JS, Forbes MS, Nolan SP. Change in endothelial cell morphology at arterial branch sites caused by a reduction of intramural stress. Atherosclerosis 1991;89:209–21. [PubMed: 1793449]

[37]. Pradhan S, Sumpio B. Molecular and biological effects of hemodynamics on vascular cells. Front Biosci 2004;9:3276–85. [PubMed: 15353357]

[38]. Thubrikar MJ, Robicsek F. Pressure-induced arterial wall stress and atherosclerosis. Ann Thorac Surg 1995;59(6):1594–603. [PubMed: 7771858]

[39]. Haga JH, Li YS, Chien S. Molecular basis of the effects of mechanical stretch on vascular smooth muscle cells. J Biomech 2007;40:947–60. [PubMed: 16867303]

[40]. Glagov S, Weisenberg E, Zarins CK, Stankunavicius R, Kolettis GJ. Compensatory enlargement of human atherosclerotic coronary arteries. N Engl J Med 1987;316:1371–5. [PubMed: 3574413]

[41]. Korshunov VA, Berk BC. Strain-dependent vascular remodeling: the “Glagov phenomenon” is genetically determined. Circulation 2004;110:220–6. [PubMed: 15226209]

[42]. Yamashita A, Shoji K, Tsuruda T, Furukoji E, Takahashi M, Nishihira K, et al. Medial and adventitial macrophages are associated with expansive atherosclerotic remodeling in rabbit femoral artery. Histol Histopathol 2008;23:127–36. [PubMed: 17999368]

[43]. von Birgelen C, Hartmann M, Mintz GS, Böse D, Eggebrecht H, Neumann T, et al. Remodeling index compared to actual vascular remodeling in atherosclerotic left main coronary arteries as assessed with long-term (< or =12 months) serial intravascular ultrasound. J Am Coll Cardiol 2006;47:1363–8. [PubMed: 16580523]

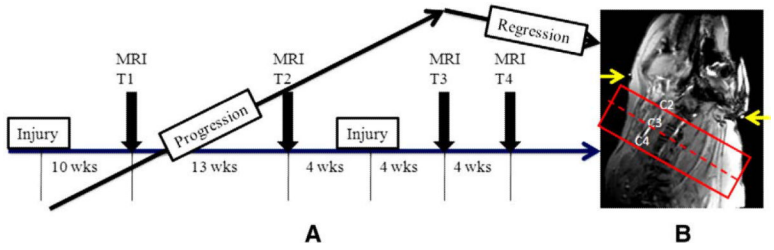

Fig. 1.

(A) Time course of the experimental study for the pigs. (B) Location of imaging volume over the neck region between second and fourth cervical vertebra. T1–T4 indicates four time points for the MRI to monitor the plaque progression. Pig 1 was evaluated only at T1 and T2, but Pig 2 and 3 underwent evaluation at all time points. The yellow arrows point to the external fiducial markers (contrast ring) attaching the neck of the pig.

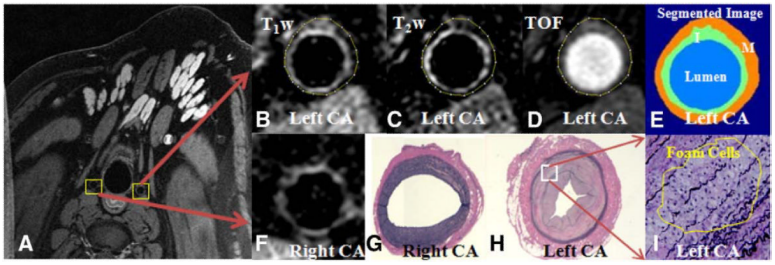

Fig. 2.

(A) Source MR images in Pig 3 to show both right and left carotid arteries. (B–E) Top panel shows three axial left carotid wall images of three contrasts: T_1-weighting, T_2-weighting and TOF, as well as the segmented image; bottom panel shows right normal carotid wall (F) and corresponding histopathological images of right (G) and left (H) carotid arteries. Strong enhancement in the neotimal wall of left carotid artery is clearly visualized. (I) zoomed histopathological images (×200) shows a small area of foam cells within the media. No foam cell is noticed within the intimal regions.

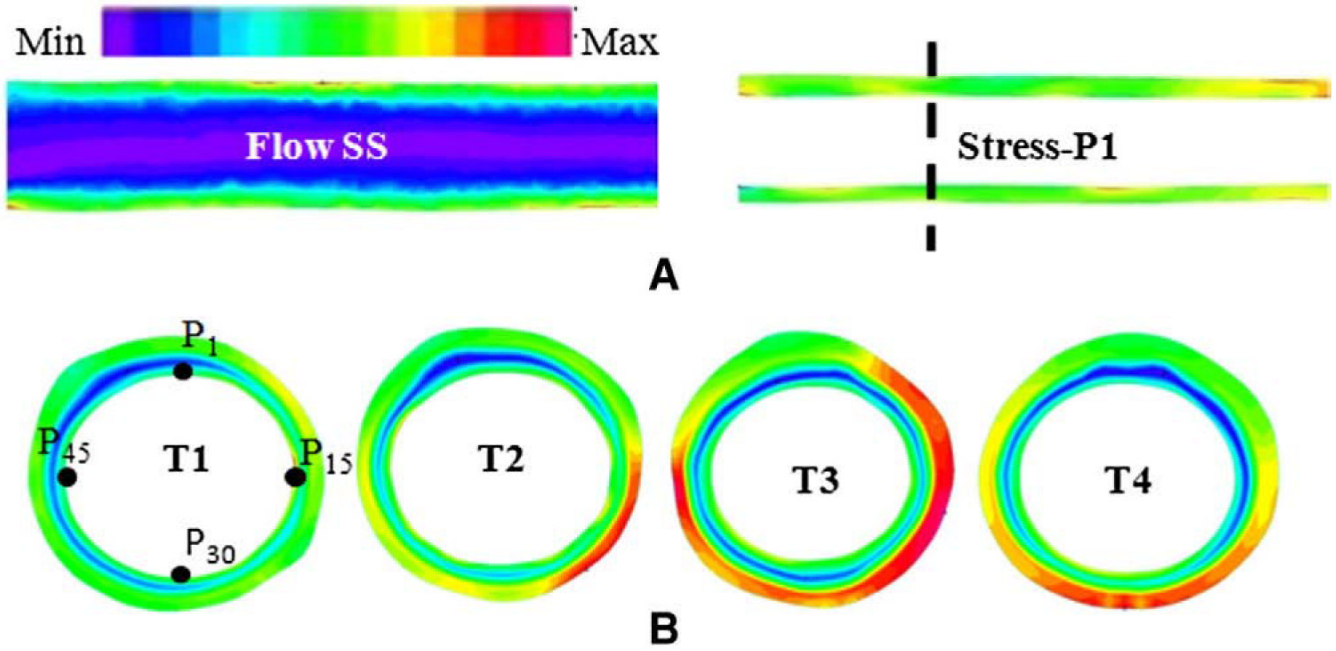

Fig. 3.

(A) Calculated flow SS and stress-P1 maps by the FSI computational model at T1. (B) One coregistered cross-sectional stress-P1 map at four time points (T1–T4). The input pressure was 93 mm Hg for all time points. The universal color bar indicates the color changes from minimum to maximum. In flow SS map, the SS values are the lowest at the center and increase toward the boundary of the vessel wall. The wall in this map is only for the purpose of demonstration (no flow SS inside the wall). The dotted line in (A) indicates the location of the cross section map in (B). The stress-P1 increased with the increases in the vessel wall size from T1 to T3 and then decreased at T4 due to the changes in plaque morphology. The point P1, P15, P30 and P45 illustrate four locations of 60 points used for data analysis. Colors are scaled from low (blue) to high values (red).

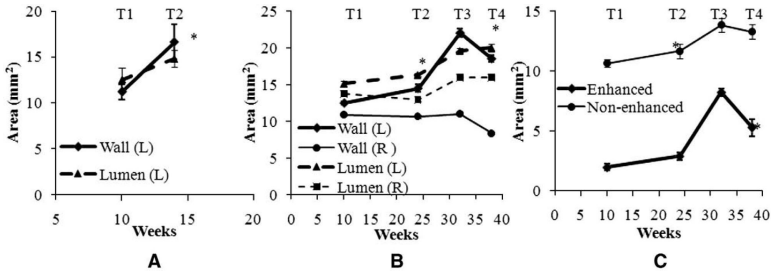

Fig. 4.

(A) Morphologic changes in the left carotid wall areas in Pig 1 from T1 to T2. (B) Morphologic changes in both left and right carotid wall areas in Pig 2 an d3 from T1 to T4. (C) Size changes in the enhanced and nonenhanced plaque areas of the left injured carotid artery in Pig 3 from T1 to T4. Left carotid arterial wall increased from T1 to T2 and then decreased from T3 to T4, whereas right arterial wall changed much less. Notice the lumen of both right and left carotid artery walls increased from T1 to T4, due to increased size of the pigs. The error bars indicate the standard errors. * P<.01 (relative to the previous time points).

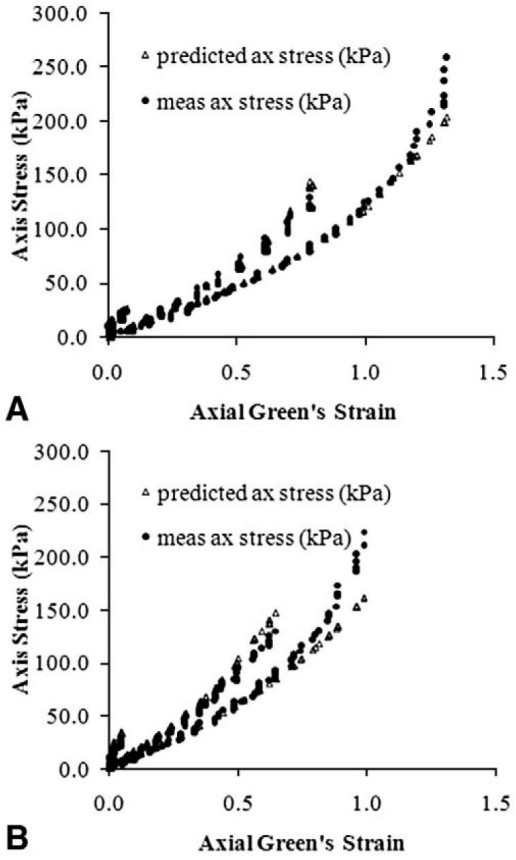

Fig. 5.

Stress vs. strain relationship for normal (A) and injured (B) carotid arterial segment in Pig 3. Stiffer arterial wall is readily to see at right one. Predicted curve is obtained from curve fitting to the Eq. (1) (see text).

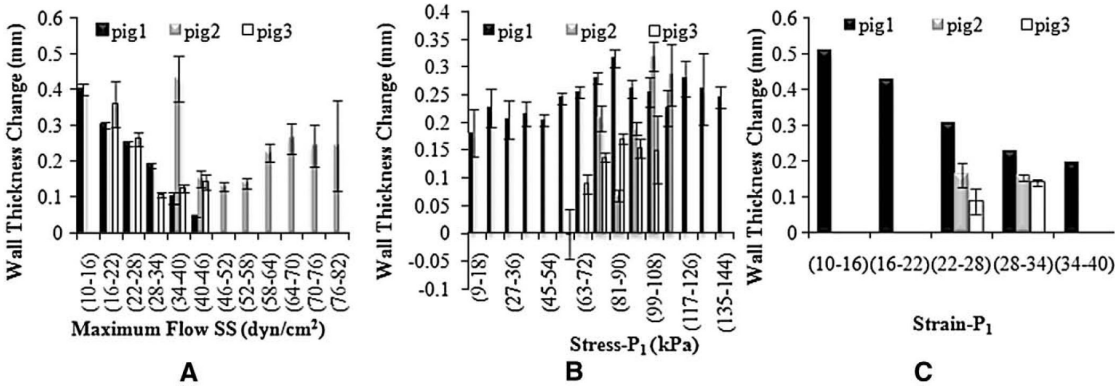

Fig. 6.

Association of the changes in carotid wall thickness and the baseline biomechanical forces during the plaque progression: flow SS (A), stress-P_1 (B) and Strain-P_1 (C). The error bars indicate the standard errors. Note that the range of wall thickness change (*y*-axis) is different in each plot, particularly between Stress-P_1 and Strain-P_1 data sets at progression period. This is because the data was divided into different categories.

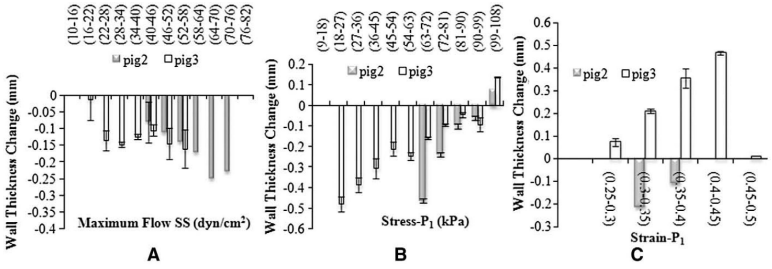

Fig. 7.

Association of the changes in carotid wall thickness and the baseline biomechanical forces during the plaque regression: flow SS (A), Stress-P_1 (B) and Strain-P_1 (C).

Table 1

Correlation coefficients between hemodynamic parameters in the category and the change in thickness of each plaque components

		Progression	Regression
Enhanced	Flow SS	−0.1 (*P*=NS) (Pig 3)	−0.68 (*P*=NS) (Pig 3)
	Stress-P1	0.86 (*P*=.01) (Pig 3)	0.96 (*P*<.0001) (Pig 3)
	Strain-P1	N/A (Pig 3)	1.0 (*P*<.0001) (Pig 3)
Non-Enhanced	Flow SS	−1.0 (*P*<.0001) (Pig 3)	0.82 (*P*=.02) (Pig 3)
		−0.11 (*P*=NS) (Pig 2)	−0.94 (*P*<.01) (Pig 2)
		−1.0 (*P*<.0001) (Pig 1)	
	Stress-P1	0.25 (*P*=NS) (Pig 3)	0.44 (*P*=NS)
		0.6 (*P*=NS) (Pig 2)	0.97 (*P*<.001) (Pig 2)
		0.62 (*P*=.014) (Pig 1)	
	Strain-P1	N/A (Pig 3)	0.7 (*P*=NS) (Pig 3)
		N/A (Pig 2)	N/A (Pig 2)
		N/A (Pig 1)	

N/A indicates insufficient data for statistical analysis.

Table 2

Vessel WR of three pigs

	Progression	**Regression**
Pig 1	1.05±0.06 to 1.21±0.10 (*P*<.01)	N/A
Pig 2	1.03±0.01 to 1.33±0.06 (*P*<.01)	1.54±0.01 to 1.44±0.03 (*P*<.01)
Pig 3	1.01±0.02 to 1.11±0.03 (*P*<.01)	1.20±0.08 to 1.18±0.07 (*P*=NS)